

Compressing the cosmological information in one-dimensional correlations of the Lyman- α forest

CHRISTIAN PEDERSEN ^{1,2,3,4} ANDREU FONT-RIBERA ^{5,3} AND NICKOLAY Y. GNEDIN ^{4,6,7}

¹*Center for Cosmology and Particle Physics, Department of Physics, New York University, New York, NY 10003, USA*

²*Center for Computational Astrophysics, Flatiron Institute, New York, NY 10010, USA*

³*Department of Physics and Astronomy, University College London, London WC1E 6BT, United Kingdom*

⁴*Fermi National Accelerator Laboratory; Batavia, IL 60510, USA*

⁵*Institut de Física d'Altes Energies (IFAE), The Barcelona Institute of Science and Technology, 08193 Bellaterra (Barcelona), Spain*

⁶*Kavli Institute for Cosmological Physics; The University of Chicago; Chicago, IL 60637 USA*

⁷*Department of Astronomy & Astrophysics; The University of Chicago; Chicago, IL 60637 USA*

ABSTRACT

Observations of the Lyman- α ($\text{Ly}\alpha$) forest from spectroscopic surveys such as BOSS/eBOSS, or the ongoing DESI, offer a unique window to study the growth of structure on megaparsec scales. Interpretation of these measurements is a complicated task, requiring hydrodynamical simulations to model and marginalise over the thermal and ionisation state of the intergalactic medium. This complexity has limited the use of $\text{Ly}\alpha$ clustering measurements in joint cosmological analyses. In this work we show that the cosmological information content of the 1D power spectrum ($P_{1\text{D}}$) of the $\text{Ly}\alpha$ forest can be compressed into a simple two-parameter likelihood without any significant loss of constraining power. We simulate $P_{1\text{D}}$ measurements from DESI using hydrodynamical simulations and show that the compressed likelihood is model independent and lossless, recovering unbiased results even in the presence of massive neutrinos or running of the primordial power spectrum.

Keywords: Lyman alpha forest (980) — Cosmology(343) — Large-scale structure of the universe(902)
— Astronomy data reduction(1861)

1. INTRODUCTION

The tightest constraints on cosmological parameters are obtained from the joint analysis of complementary probes, with different sensitivity to cosmological parameters. A common approach is to combine observations of the cosmic microwave background (CMB) with late-time probes of large-scale structure (LSS), such as galaxy clustering or weak lensing (Planck Collaboration et al. 2020; Alam et al. 2021; Abbott et al. 2022). An alternative probe of LSS is the Lyman- α ($\text{Ly}\alpha$) forest, a series of absorption features in the spectra of $z > 2$ quasars, caused by intervening neutral hydrogen along the line-of-sight.

Cosmological analysis of the $\text{Ly}\alpha$ forest is driven by large spectroscopic surveys, such as the Baryon Oscillation Spectroscopic Survey (BOSS, (Dawson et al. 2013)) and its extension eBOSS (Dawson et al. 2016), which

between 2009 and 2019 observed $\sim 200,000$ $\text{Ly}\alpha$ forest quasars. In 2021, the Dark Energy Spectroscopic Instrument (DESI) (Aghamousa & et al. ????) started a five-year program to survey a third of the sky and obtain spectra of $\sim 800,000$ $\text{Ly}\alpha$ forest quasars. The main goal of these quasar surveys is to measure the 3D correlations in the $\text{Ly}\alpha$ forest and to provide accurate measurements of the Baryon Acoustic Oscillations (BAO) feature to study the expansion of the universe (du Mas des Bourboux et al. 2020). The same dataset, however, can be used to measure correlations along the line of sight, known as the 1D flux power spectrum ($P_{1\text{D}}$), a unique window to study the clustering of matter on megaparsec scales (Chabanier et al. 2019a).

Cosmological analyses of the $P_{1\text{D}}$ are particularly powerful in combination with CMB measurements due to the large “lever arm” between the two measurements, and these joint analyses have historically provided some of the tightest constraints on the sum of the neutrino masses, and on the shape of the primordial power spectrum of density fluctuations (Phillips et al. 2001; Verde

et al. 2003; Spergel et al. 2003; Viel et al. 2004; Seljak et al. 2005, 2006; Bird et al. 2011; Palanque-Delabrouille et al. 2015a,b, 2020).

Massive neutrinos are known to affect the growth of structure by suppressing the late-time clustering of matter on scales smaller than their free-streaming length (Lesgourgues & Pastor 2006). The P_{1D} alone is unable to constrain neutrino masses due to parameter degeneracies (Pedersen et al. 2020), but when combined with the early-time, large-scales measurements from the CMB one can break these degeneracies. In the next few years, and in combination with CMB measurements, several LSS probes will be able to detect the impact of massive neutrinos, even if the sum of the masses is near the minimum of $\Sigma m_\nu = 0.06$ eV allowed by oscillation experiments (Font-Ribera et al. 2014).

At the same time, inflationary models generically predict that the primordial power spectrum of fluctuations should have small deviations from a power law, often parameterised as a *running* of the spectral index. Due to the wide lever arm between the large scale fluctuations probed by *Planck* and the small scales accessed by the P_{1D} , the Ly α forest is one of the most promising avenues towards tightening the constraints on inflationary models which produce a measurable running of the spectral index (Font-Ribera et al. 2014).

Unfortunately for cosmologists, the statistical properties of the Ly α forest also depend on the thermal and ionisation history of the intergalactic medium (IGM) (McQuinn 2016)¹. This has two consequences that complicate P_{1D} analyses. First, it means that we need to run expensive hydrodynamical simulations in order to make accurate predictions for a given model. Second, it means that we need to add multiple nuisance parameters in our cosmological inference, and to carefully marginalise over them to obtain robust cosmological constraints.

In the last few years, several groups have attempted to tackle the first problem, introducing new tools to *emulate* P_{1D} for parameters that are not covered by the relatively small suite of simulations available (Walther et al. 2019; Bird et al. 2019; Rogers et al. 2019; Takhtaganov et al. 2021; Rogers & Peiris 2021a; Pedersen et al. 2021). In this publication, we will use the LaCE² emulator presented in Pedersen et al. (2021), and focus on the second problem: the high-dimensionality of the parameter space sampled, and the attractive possibility of dramatically reducing the dimensionality of the P_{1D} likelihood into a small number of parameters describing the linear

matter power spectrum, without introducing biases or losing relevant information.

The idea of compressing the P_{1D} likelihood into a handful of parameters describing the linear power spectrum is not new. Indeed, the first cosmological studies of the Ly α forest focused on recovering the matter power spectrum (Croft et al. 1998; McDonald et al. 2000; Croft et al. 2002; Gnedin & Hamilton 2002), and the two-parameter (amplitude and slope) parameterisation we focus on in this work was already used 20 years ago (McDonald et al. 2000). However, most recent P_{1D} analyses from BOSS and eBOSS surveys have only presented their results in terms of direct fits to the traditional Λ CDM parameters (Borde et al. 2014; Palanque-Delabrouille et al. 2015a,b, 2020), with strong dependence on the priors chosen. This has made it difficult for other groups to include these powerful results into combined cosmological analyses. If the Ly α forest constraints from P_{1D} could be accurately and losslessly represented by just the amplitude and a local slope at a conveniently chosen pivot scale, it would significantly simplify the combination of Ly α forest measurements with other cosmological probes.

Motivated by the latest P_{1D} measurements from eBOSS, the start of the DESI survey, and the recent developments in emulation techniques, in this publication we review the compression of the P_{1D} likelihood. Note that similar discussions are also happening in the context of analysis of the galaxy power spectrum, in particular regarding the information content in measurements of redshift space distortions (Hamann et al. 2010; Ivanov et al. 2020; d’Amico et al. 2020; Brieden et al. 2021).

We will start in Section 2 with a description of the simulated data, a summary of the emulator used, and the parameterisation of the likelihood. In Section 3 we present cosmological constraints from simulated P_{1D} data, and discuss the impact of priors and model dependency of the results. In Section 4 we present joint fits when combining the P_{1D} with an approximated CMB likelihood, and show that the P_{1D} likelihood can be efficiently compressed into two parameters without any loss of information. Finally in Section 5 we discuss our findings.

2. METHODOLOGY

We discuss here the Ly α forest P_{1D} likelihood, including an overview of the emulator used to make theoretical predictions (based on (Pedersen et al. 2021)), a description of the mock dataset, and a discussion of the parameterisation of the likelihood.

2.1. Simulations

¹ This also makes the Ly α forest, specially at $z > 5$, a key probe of reionisation, but we do not discuss this in this work.

² <https://github.com/igmhub/LaCE>

We begin by describing the simulations used in the analysis, which fall into two categories. First, a set of *training* simulations are used to construct the emulator. Second, a small number of *test* simulations are run, to represent mock P_{1D} measurements in a variety of different cosmologies, and are used to test and validate our analysis pipeline. Both the training and most of the test simulations were presented in Pedersen et al. (2021), where we also described and tested the emulation framework. Here we give an overview of the simulations, and refer the reader to Pedersen et al. (2021) for a more detailed description.

The simulations were run in `MP-Gadget`³ (Feng et al. 2018), a `TreeSPH` code based on `Gadget-2` (Springel 2005). All simulation boxes had a size of $L = 67.5$ Mpc and 768^3 gas and cold dark matter (CDM) particles. The initial conditions were generated with `MP-GenIC` at $z = 99$, with Fourier modes that had random phases but fixed initial amplitudes (Angulo & Pontzen 2016; Anderson et al. 2019; Villaescusa-Navarro et al. 2018; Pedersen et al. 2021). In order to further reduce cosmic variance, for each model (both in the training and test sets) we ran a pair of simulations with inverted phases, and each quantity estimated from the simulations is taken as the average of the pair.

We output 11 snapshots, equally spaced in redshift between $z = 2$ and $z = 4.5$. To produce mock Ly α forest spectra from each snapshot, we use `fake_spectra`⁴ (Bird 2017) to calculate a 2D grid of 500^2 transmission skewers from each snapshot, with a line-of-sight resolution of 0.05 Mpc. The cosmological and astrophysical parameters used in both the training and test simulations are listed in Table 1.

2.2. Emulator

We provide a brief overview of the emulator parameters and framework. We use the `LaCE`⁵ framework presented in Pedersen et al. (2021), and refer the reader to this reference for a more complete description. `LaCE` uses a Gaussian Process emulator⁶ to predict P_{1D} as a function of six parameters: the dimensionless amplitude (Δ_p^2) and slope (n_p) of the linear power spectrum around a pivot scale of $k_p = 0.7$ Mpc⁻¹; the mean transmitted flux fraction (or mean flux, \bar{F}); a thermal broadening scale defined in comoving units (σ_T^{com}), set by the temperature of the gas at mean density; the slope of the temperature-density relation (γ); the filtering length in

	Training set	<i>Central</i>	<i>Neutrino</i>	<i>Running</i>
$A_s (\times 10^{-9})$	[1.35–2.71]	2.006	2.251	2.114
n_s	[0.92–1.02]	0.9676	0.9676	0.9280
α_s	0.0	0.0	0.0	0.015
Ω_m	0.316	0.316	0.324	0.316
Σm_ν (eV)	0.0	0.0	0.3	0.0
$\Delta_p^2(z = 3)$	[0.25–0.45]	0.35		
$n_p(z = 3)$	–[2.35–2.25]	–2.30		
z_{rei}	[5.5–15]	10.5		
H_A	[0.5–1.5]	1.0		
H_S	[0.5–1.5]	1.0		

Table 1. Cosmological and astrophysical parameters for the training and test simulations. The limits of the Latin hypercube for the training simulations are shown in the left column, where only the primordial power spectrum and astrophysical parameters are varied. The primordial parameters A_s and n_s here are defined at the CMB pivot scale of $k = 0.05$ Mpc⁻¹. The *Central*, *Neutrino* and *Running* simulations are constructed such that they have the same small scale linear matter power spectrum (Δ_p^2 and n_p) at $z = 3$. For all simulations, we fix $\omega_c = 0.12$, $\omega_b = 0.022$ and $h = 0.67$.

inverse comoving units (k_F^{com}), a proxy for gas pressure. Note that whilst the P_{1D} is naturally observed in velocity units, the above quantities are all defined in comoving units in the emulator. The motivation for this is so that the simulated P_{1D} is estimated at a fixed set of wavenumbers for snapshots at all redshifts.

We train the emulator using 30 pairs of simulations described in Table 1. These simulations explore different thermal and reionisation histories by varying z_{rei} , H_A , and H_S , which control the redshift of reionisation and the heating rates of the gas as rescalings around a fiducial model from Haardt & Madau (2012) (see Pedersen et al. (2021) for more detail). The simulations have different amplitudes and slopes of the primordial power spectrum (A_s , n_s), but have the same value for the physical densities of CDM ($\omega_c = \Omega_c h^2$) and baryons ($\omega_b = \Omega_b h^2$), the same value of H_0 , and do not include massive neutrinos. All 11 snapshots from all 30 models are used simultaneously, for a total of 330 points in the training sample.

In the implementation of the emulator presented in Pedersen et al. (2021), the Ly α P_{1D} was emulated directly on a grid of comoving wavenumbers. Because of the limited box size of our simulations, the P_{1D} measurements on large scales are affected by cosmic variance. Given that each simulation was run with the same random seed, there are random noise spikes in the power spectrum that align at the same comoving wavenumbers in each simulation used to train the emulator. When it

³ <https://github.com/MP-Gadget/MP-Gadget>.

⁴ <https://github.com/sbird/fake-spectra>.

⁵ <https://github.com/igmhub/LaCE>.

⁶ We use the Python implementation `GPpy` (GPpy since 2012).

came to testing the pipeline on simulated mock data with a different background evolution, we found that these noise spikes are interpreted by the emulator as sharp features in the power spectrum, artificially enhancing the emulator sensitivity to changes in cosmology. This is due to the fact that the likelihood evaluation is performed in velocity units, which require a conversion from comoving units using $H(z)$. The pipeline would therefore try and find the $H(z)$ which would align the noise spikes in the observed data with the noise spikes in the training set, with two consequences. When running on mock simulations with the same training seed, the pipeline is artificially sensitive to the conversion between comoving and velocity units, and therefore $H(z)$, due to the presence of these sharp features. When running on mock simulations with a different random seed, the pipeline struggles to return the correct cosmology, as the likelihood maximisation is dominated by the incentive to align the different noise features.

In order to remove residual noise in the measurements of P_{1D} , we fit a 4th order polynomial⁷ to the logarithm of P_{1D} as a function of the logarithm of wavenumber, using scales $k_{\parallel} < 8 \text{ Mpc}^{-1}$:

$$\log P_{1D}(k_{\parallel}) = \sum_{n=0}^4 c_n (\log k_{\parallel})^n . \quad (1)$$

Instead of predicting directly P_{1D} the emulator now predicts the five coefficients c_n of this polynomial, that can later be used to predict P_{1D} on all scales. The use of fitting functions, such as polynomials or principle component analysis is a standard practice to reduce noise in emulators, such as in the ‘‘Coyote’’ emulator (Lawrence et al. 2010) as well as in early analyses of P_{1D} (McDonald et al. 2005).

The variance on the emulated coefficients ($\sigma_{c_n}^2$) can be used to obtain an estimate for the variance of the emulated P_{1D} :

$$\left(\frac{\sigma_{P_{1D}}}{P_{1D}}\right)^2 = \sum_{n=0}^4 \sigma_{c_n}^2 (\log k_{\parallel})^{2n} . \quad (2)$$

We discuss the impact of cosmic variance on emulator predictions in Appendix B.

2.3. Mock data

In order to test our analysis pipeline, we have generated three synthetic datasets (or *mocks*) for models that are not included in the training set of the emulator:

- *Central* simulation: this is the simplest case, a simulation without massive neutrinos or running, with the same background expansion as was used in all training simulations, and a primordial power (A_s, n_s) corresponding to the centre of the Latin Hypercube used to setup the training set.
- *Neutrino* simulation: a simulation with $\Sigma m_{\nu} = 0.3 \text{ eV}$, where the cosmological constant (Λ) has been lowered to compensate the increase in the total matter density. The amplitude of the primordial power is also $\sim 10\%$ larger to compensate the suppression of power caused by massive neutrinos. In Pedersen et al. (2021) we used this simulation to show that we could recover unbiased predictions in cosmologies with massive neutrinos, even when the emulator was trained exclusively with simulations with massless neutrinos.
- *Running* simulation: a simulation with the same cosmology than the *Central* simulation, except that its primordial power spectrum has a non-zero running of $\alpha_s = 0.015$. The other parameters describing the primordial power (A_s, n_s) have been modified to compensate the change in running and have the same linear power around the pivot scale used in the emulator ($k_p = 0.7 \text{ Mpc}^{-1}$, see Table 1).

We start by running a pair of simulations (with inverted phases) for each of the three test models. From each of their 11 snapshots we measure P_{1D} , in comoving units, and fit a 4th order polynomial as described in Section 2.2 above. In order to roughly simulate the statistical power of DESI, we use a rescaled version of the SDSS DR14 covariance matrix of Chabanier et al. (2019b), where all elements are divided by 5 to approximately take into account the difference in the number of spectra between SDSS DR14 and DESI⁸. As is common in P_{1D} measurements, the band powers presented in Chabanier et al. (2019b) are defined in velocity units. At each redshift we compute $H(z)/(1+z)$ using the simulation cosmology to translate these into wavenumbers in comoving units.

2.4. Likelihood

We use a Gaussian likelihood, naturally decomposed into 11 independent sub-likelihoods, one for each snapshot (redshift bin). The covariance matrix is the sum

⁷ This setting performed better than 3rd or 5th order polynomials, but we did not explore other functions.

⁸ A more detailed forecast should also take into account the differences in pixelisation, spectral resolution and signal to noise, but we leave this for future work.

of the data covariance and an extra term describing the uncertainty in the emulator predictions, computed with Equation 2. The typical emulator uncertainty is smaller than 1% for models near the centre of our training set, and it only has a minor impact on likelihood evaluations around the best-fit values of our analyses. However, it can be larger than 10% when evaluating the likelihood near the convex hull of our training sample.

Different sub-sections in Section 3 and Section 4 use a different number of free cosmological parameters, including: the amplitude (A_s), slope (n_s) and running (α_s) of the primordial power spectrum at the usual CMB pivot scale of $k_s = 0.05 \text{ Mpc}^{-1}$; the physical densities of baryons ($\omega_b = \Omega_b h^2$) and of CDM ($\omega_c = \Omega_c h^2$); the sum of the neutrino masses (Σm_ν); the Hubble parameter H_0 ; the angular acoustic scale of the CMB (θ_{MC}).

We use four functions to describe thermal and ionisation history of the IGM: the effective optical depth as a function of redshift $\tau(z) = -\log \bar{F}(z)$, the thermal broadening scale (in km s^{-1}) at mean densities $\sigma_T^{\text{vel}}(z)$, the slope of the temperature-density relation $\gamma(z)$ and the filtering / pressure scale $k_F^{\text{vel}}(z)$ (in s km^{-1}). Following Pedersen et al. (2021), we measure each of these functions from the *Central* simulation, and use two parameters, α_X and β_X , to describe a power law rescaling for each of the four functions. Here the subscript X refers to one of the four IGM parameters. For instance, the thermal broadening scale, $\sigma_T^{\text{vel}}(z)$ is parameterised as

$$\ln \sigma_T^{\text{vel}}(z) = \ln \sigma_T^{\text{vel}}(z)|_{\text{cen}} + a_{\sigma_T} + b_{\sigma_T} \ln \frac{1+z}{1+3}, \quad (3)$$

where $\sigma_T^{\text{vel}}(z)|_{\text{cen}}$ is the thermal broadening scale in the *Central* simulation. Therefore we use a total of 8 nuisance parameters related to IGM physics.

There is no guarantee that this simple parameterisation is accurate enough to do an analysis on real data, but it should be flexible enough to test the compression of the likelihood in a realistic setting. As described in Table 2, we use combined priors: each parameter is allowed to vary within a given range of values (top hat prior) and an additional weak Gaussian prior is applied to all parameters; the actual prior is a product of the two.

In the next sections we will discuss constraints on two derived parameters that are able to capture most of the cosmological information in $P_{1\text{D}}$: the (dimensionless) amplitude and slope of the linear power spectrum at

Parameter	Range allowed	Gaussian prior
$A_s (\times 10^{-9})$	[1.0 – 3.2]	$\mathcal{N}(2.1, 1.1)$
n_s	[0.89 – 1.05]	$\mathcal{N}(0.965, 0.08)$
α_s	[−0.8 – 0.8]	$\mathcal{N}(0.0, 0.8)$
ω_b	[0.018 – 0.026]	$\mathcal{N}(0.022, 0.004)$
ω_c	[0.10 – 0.14]	$\mathcal{N}(0.12, 0.02)$
Σm_ν (eV)	[0.0 – 1.0]	$\mathcal{N}(0.0, 0.5)$
H_0	[50 – 100]	$\mathcal{N}(67.0, 25.0)$
$\theta_{\text{MC}} (\times 10^{-3})$	[9.9 – 10.9]	$\mathcal{N}(10.4, 0.5)$
a_τ	[−0.1 – 0.1]	$\mathcal{N}(0.0, 0.05)$
b_τ	[−0.2 – 0.2]	$\mathcal{N}(0.0, 0.1)$
a_{σ_T}	[−0.4 – 0.4]	$\mathcal{N}(0.0, 0.2)$
b_{σ_T}	[−0.4 – 0.4]	$\mathcal{N}(0.0, 0.2)$
a_γ	[−0.2 – 0.2]	$\mathcal{N}(0.0, 0.1)$
b_γ	[−0.4 – 0.4]	$\mathcal{N}(0.0, 0.2)$
a_{k_F}	[−0.2 – 0.2]	$\mathcal{N}(0.0, 0.1)$
b_{k_F}	[−0.4 – 0.4]	$\mathcal{N}(0.0, 0.2)$

Table 2. Priors used for the cosmological parameters (top), and for the nuisance parameters describing the thermal and ionisation history of the IGM (bottom). All parameters have a limited range of values allowed, and a Gaussian prior.

a pivot point $k_\star = 0.009 \text{ s km}^{-1}$ and redshift $z_\star = 3$ ⁹:

$$\Delta_\star^2 = \frac{k_\star^3 P_L(k_\star, z_\star)}{2\pi^2}, \quad (4)$$

$$n_\star = \left. \frac{d \ln P_L(k, z)}{d \ln k} \right|_{k_\star, z_\star} \quad (5)$$

where $P_L(k, z)$ is the linear power spectrum *in velocity units*. It is important to highlight that these parameters are defined in velocity units, since $P_{1\text{D}}$ measurements are also presented in velocity units and parameters defined in comoving units would be model dependent.

Let us finish this section by summarising the steps needed to make a likelihood evaluation:

- Given a set of cosmological parameters, we use the Boltzman solver **CAMB** (Lewis et al. 2000) to make predictions for $P_L(z, k)$ and $H(z)$ at all redshifts and scales.
- For each redshift z_i in our mock $P_{1\text{D}}$ measurement, we compute the value of the amplitude (Δ_p^2) and slope (n_p) of the linear power, $P_L(z_i, k)$, around the pivot point $k_p = 0.7 \text{ Mpc}^{-1}$. These are two of the six parameters that will be passed to the emulator to get a prediction of $P_{1\text{D}}$ at z_i .

⁹ This pivot scale was found in McDonald et al. (2005) to be optimal for their dataset, but it might be sub-optimal for other surveys.

- The other four parameters (\bar{F} , σ_T^{com} , γ , k_F^{com}) are computed from the eight nuisance parameters and the four IGM-related functions measured from the *Central* simulation. For instance, we use Equation 3 to compute the thermal broadening scale (σ_T^{vel}) in velocity units at redshift z_i , and the comoving scale passed to the emulator is $\sigma_T^{\text{com}} = \sigma_T^{\text{vel}}(1 + z_i)/H(z_i)$.
- For each redshift, we ask the emulator to predict the P_{1D} corresponding to the six emulator parameters computed above. The emulator prediction is in comoving units, and we use $H(z_i)$ to translate it to velocity units.
- The emulator also returns an uncertainty associated to the prediction, that we add to the data covariance (after translating the emulator covariance to velocity units).
- We use these ingredients to compute a Gaussian likelihood, and multiply it by the prior probability described above.

We use `emcee` (Foreman-Mackey et al. 2013) to run Monte Carlo Markov Chains, and we use `GetDist` (Lewis 2019) to make contours plots with marginalised posteriors.

3. COSMOLOGICAL INFORMATION IN THE Ly α P_{1D}

In this section we follow the methodology described in Section 2 to fit cosmological parameters from a synthetic measurement of P_{1D} . We refer to these as *direct fits*.

In Figure 1 we show the marginal constraints on cosmological parameters when analysing mock data from the *Central* simulation. In the standard analysis (blue), we vary five cosmological parameters and eight nuisance parameters describing the IGM that are not shown. For comparison, the black lines show the constraints from the priors described in Table 2.

It is clear that Ly α P_{1D} alone cannot measure well these five cosmological parameters, and that the results strongly depend on the choice of priors (the impact of the prior choice is discussed in Appendix A). For instance, the constraints on A_s are affected by the maximum value allowed by the prior, and its lower bound is a consequence of the prior on neutrino masses Σm_ν being positive.

On the top right corner of Figure 1 we also show the marginal posteriors for the two derived parameters describing the linear power spectrum at $z = 3$ (Equations 4 and 5). It is clear that adding P_{1D} reduces dramatically the area of the prior contours. In the next sections we

will refer to these as the *compressed* parameters, since they are able to compress most of the cosmological information contained in the Ly α P_{1D} .

3.1. Fixed template and fiducial cosmology

The red contours in Figure 1 show a simplified version of the analysis where only the primordial power parameters (A_s , n_s) and the eight IGM parameters are varied. In other words, we use a fixed *template*¹⁰ for the linear power $P_L(z, k)$ and rescale it with these two parameters. This analysis is significantly faster than the standard analysis, since we only need to call CAMB a single time to compute the transfer function for the fiducial cosmology.

The *template* analysis can be seen as an analysis with infinitely tight priors on the other cosmological parameters (ω_c , H_0 , Σm_ν). While the constraints on the traditional cosmological parameters (A_s , n_s) are strongly affected by this change in the priors, the constraints on the compressed parameters (Δ_\star^2 , n_\star , top right panel) remain the same.

In this particular realisation of the analysis, we have used a template computed with the same cosmology that was used to run the simulation. Even in the standard analysis (blue contours in Figure 1) we had to assume a value for the baryon density ($\omega_b = 0.022$). We will use the term *fiducial cosmology* to refer to the cosmological parameters that are being kept fixed in the analysis. Obviously in a real analysis the true cosmology is not known, and so we next test the effect of changing this fiducial cosmology on our results.

In the top panels of Figure 2 we redo the *template* analysis when using different fiducial cosmologies, with the wrong CDM density (in red) or the wrong sum of the neutrino masses (in blue). While there is a clear bias on the primordial power parameters (left), the compressed parameters are much less affected by the choice of fiducial cosmology.

The bottom panels of the same figure show a *template* analysis for the three test simulations described in Table 1. In all three analyses we use the *Central* cosmology as our fiducial cosmology. As can be seen in the left bottom panel, this results in biased posteriors for the primordial power parameters in the *Neutrino* and *Running* simulations (stars identify the true values used in each simulation). However, the marginal posteriors of the compressed parameters are again recovered success-

¹⁰ This term is commonly used in redshift-space distortion (RSD) analyses of galaxies to refer to analyses with fixed transfer functions (Alam et al. 2021).

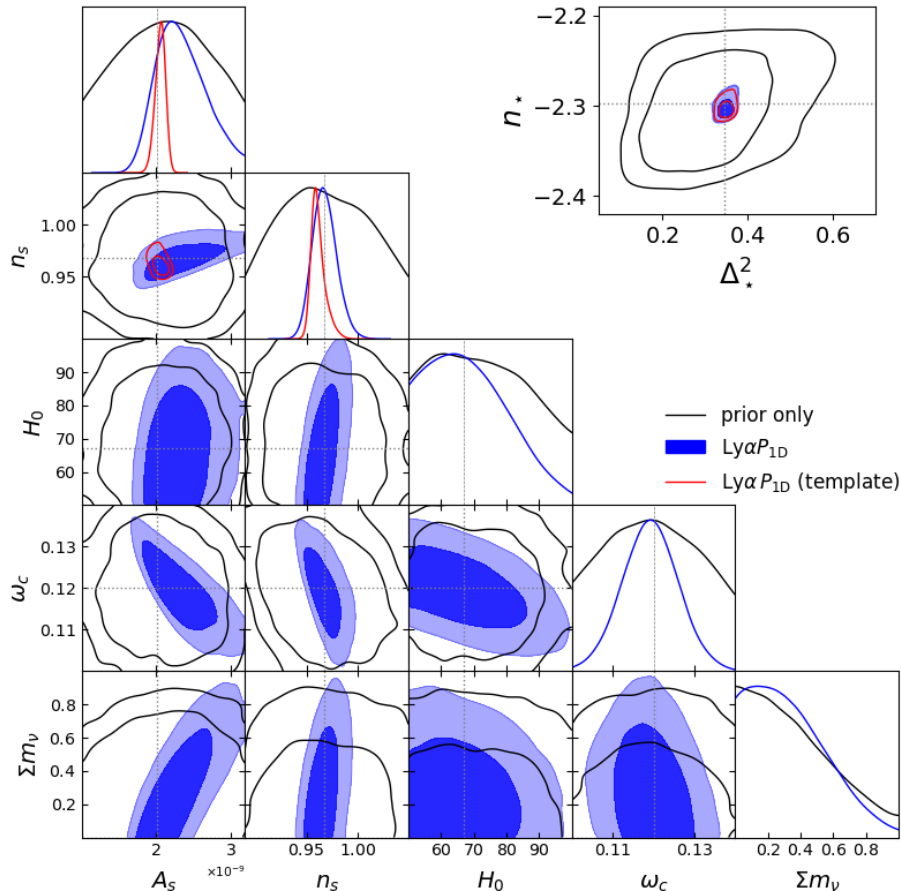


Figure 1. Direct fits to cosmological parameters from a mock P_{1D} measurement from the *Central* simulation. We show the marginal posteriors on the five cosmological parameters that are being sampled. The top-right panel shows the marginal posteriors on the two derived parameters that will be used to compress the likelihood. Black lines correspond to running the analysis with only the prior, and dotted gray lines show the true values used to generate the mock. The blue contours show constraints from the P_{1D} with all five cosmology parameters free. In the red contours, we show results where we use a *template* cosmology, and fix all cosmology parameters to the values in the *Central* simulation, except A_s and n_s which are kept free. We investigate the dependence of our posteriors on this choice of template in Figure 2. For concision, we omit contours for the IGM parameters.

fully (right bottom panel). These marginal posteriors in the bottom right panel will be used in the next section.

4. JOINT ANALYSIS WITH CMB

In the previous sections we discussed cosmological fits from the $\text{Ly}\alpha P_{1D}$ alone, with only weak priors on cosmological parameters. We showed that we can measure very well the amplitude (Δ_\star^2) and slope (n_\star) of the linear power spectrum around $z_\star = 3$ and $k_p = 0.009 \text{ s km}^{-1}$, and that the constraints on these *compressed* parameters were unbiased, and do not depend on our choice of priors or fiducial cosmology.

In this section we discuss joint cosmological analysis with anisotropies in the Cosmic Microwave Background (CMB). CMB and P_{1D} measurements are very complementary, since together they cover a very wide range of scales and redshifts. This has made these joint analy-

ses very popular in the past (Phillips et al. 2001; Verde et al. 2003; Spergel et al. 2003; Seljak et al. 2005, 2006; Palanque-Desabrouille et al. 2015a,b, 2020), and they are forecasted to provide some of the tightest constraints on the sum of the neutrino masses and on the running of the spectral index from future surveys (Font-Ribera et al. 2014).

Instead of using an actual CMB likelihood, for simplicity we use a Gaussian likelihood on the relevant cosmological parameters. The Gaussian likelihood uses a covariance matrix obtained from the official *Planck* chains¹¹. The centre of the Gaussian has been set to the values used in the different test simulations described in Sec-

¹¹ For chains with massive neutrinos, we have computed the covariance around its best-fit value ($\Sigma m_\nu = 0$) and not around its mean.

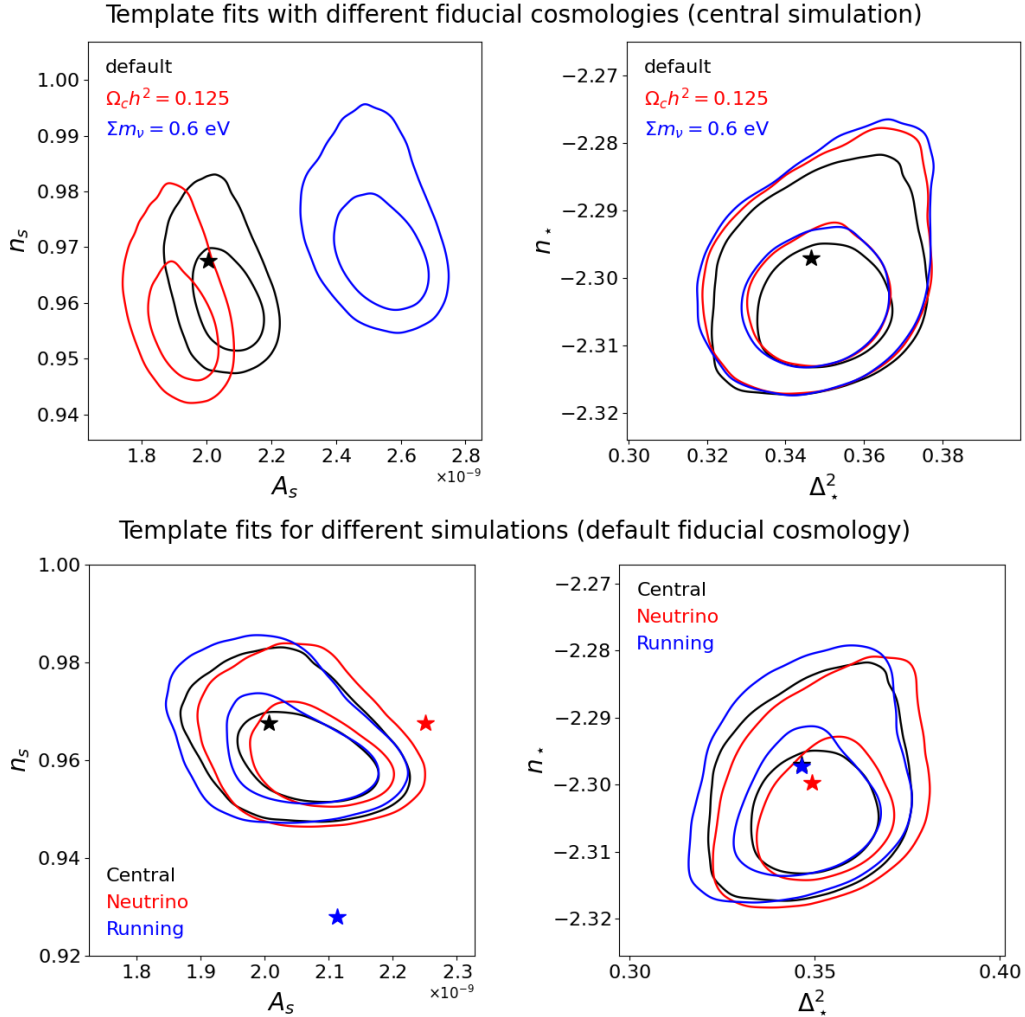


Figure 2. Top panels show marginal constraints on the primordial power parameters (left) and on the compressed parameters (right), when analysing the *Central* simulation with different fiducial cosmologies. The fiducial cosmology in the *default* analysis is the same one that was used to run the *Central*, and stars mark the true value used in the simulation. When using a different fiducial cosmology, with an incorrect value of the CDM density (red) or neutrino masses (blue) we get biased constraints on primordial power parameters. On the other hand, the constraints on the compressed parameters are much less affected by the choice of fiducial cosmology. The bottom panels show equivalent constraints for the three test simulations, when analysed with the *Central* cosmology as fiducial. Note that the *Central* (black) and *Running* (blue) simulations have the same values for the compressed parameters, but very different values for the primordial power spectrum (including different value of the running α_s).

tion 2. The approximated CMB likelihood can be seen in solid black contours in Figures 3 (free neutrino mass) and 4 (free running).

The results in Figure 3 are from a joint analysis of the CMB and our mock P_{1D} from the *Neutrino* simulation, when varying 6 cosmological parameters (A_s , n_s , $\omega_b = \Omega_b h^2$, $\omega_c = \Omega_c h^2$, Σm_ν and θ_{MC}), with the priors described in Table 2. Even though we sample θ_{MC} , we plot the contours for H_0 , computed as a derived parameter.

The blue contours show a joint fit using the direct P_{1D} likelihood, i.e., we have varied at the same time the

cosmological parameters and the 8 nuisance parameters that were also used in Section 3 to describe the uncertainties in the physics of the IGM.

The red contours, on the other hand, use the marginal posterior on the linear power parameters (Δ_\star^2 , n_\star) obtained from the Ly α P_{1D} alone. In more detail, to obtain the red contours we:

- Run a *template* fit to the Ly α P_{1D} alone, varying 8 IGM parameters and 2 cosmological parameters (A_s , n_s), as described in Section 3.

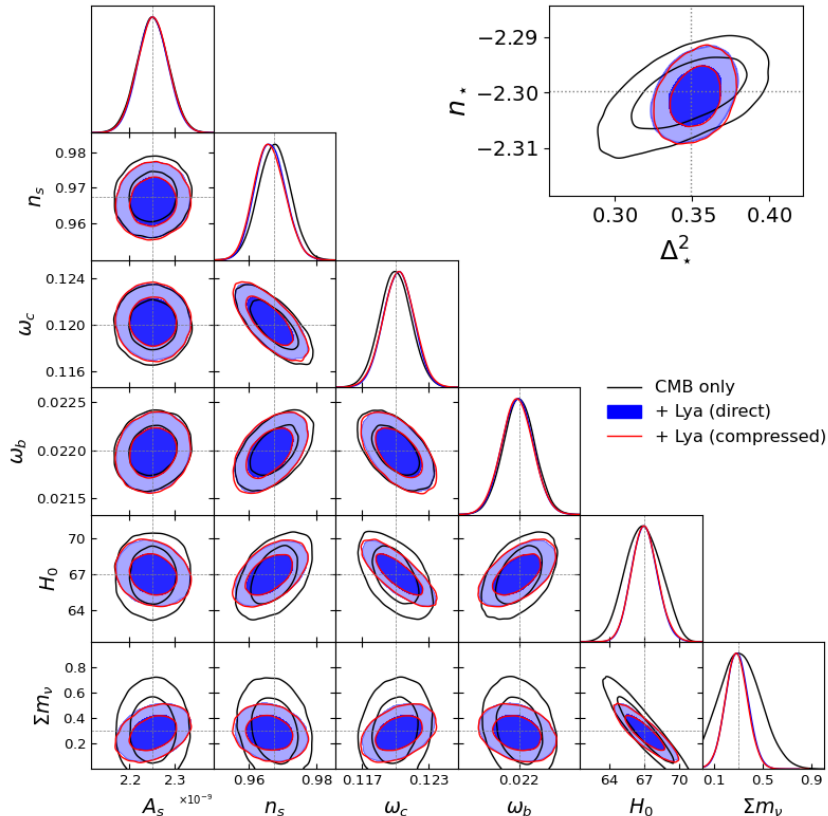


Figure 3. Cosmological constraints from CMB + Ly α P_{1D} , for mock data from the *Neutrino* simulation. Blue contours use a direct P_{1D} likelihood, while red contours use the marginal posterior on linear power parameters (Δ_\star^2, n_\star). Black contours show the CMB-only results, with the grey dashed lines representing the values in the mock simulation. The primordial power is assumed to have no running in this analysis.

- Use a Kernel Density Estimator (KDE, from SciPy (Virtanen et al. 2020)) to model the marginal posteriors on the two compressed parameters (Δ_\star^2, n_\star), shown in the bottom right panel of Figure 2.
- Run a joint analysis of CMB and the marginal Ly α P_{1D} posterior, varying 6 cosmological parameters ($A_s, n_s, \omega_b, \omega_c, \Sigma m_\nu$ and θ_{MC}). It is important to note that in this last step one does not need to use an emulator, or worry about the nuisance parameters describing the IGM; these have already been marginalised over in the previous steps.

It is remarkable that in both cases we recover the true value for the sum of the neutrino masses, even though our emulator was constructed from simulations that assume massless neutrinos. It is also remarkable how similar are the joint constraints when using the *direct* (blue) and *compressed* (red) likelihoods. This implies that there is negligible loss of cosmological information when compressing the P_{1D} into marginal constraints on the linear power spectrum.

In Figure 4 we present a similar analysis for the *Running* simulation, where we have assumed that neutrinos are massless but we have explored models with running of the spectral index α_s . Here again we recover the right cosmology, and both approaches give very consistent results.

The effect on posteriors of including Ly α forest information is slightly different in Figures 3 and 4. Whilst we do not include a figure for this, in the case of a simple flat Λ CDM model, the constraints from the CMB alone on Δ_\star^2 and n_\star are already very good, and the Ly α forest does not provide a significant improvement. It is in the analysis of extended models, such as the two we consider in this work, that the contribution from Ly α forest becomes important. In the case of free neutrino mass, the improvement is mostly in Δ_\star^2 . This is because free neutrino mass opens up a degeneracy in the amplitude of the late-time power spectrum obtained from CMB-only analysis, and including Ly α forest information breaks this degeneracy. For the case of free α_s , the information from a smaller pivot scale is essential in breaking the degeneracy between α_s and n_\star .

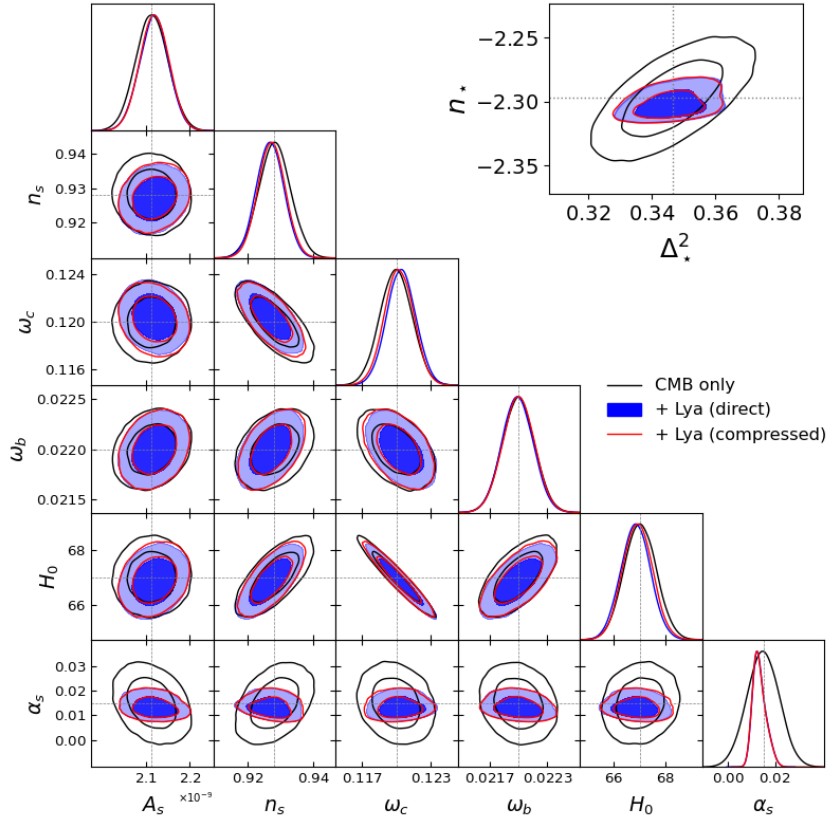


Figure 4. Same as Figure 3, except now using the mock data from the *Running* simulation. Neutrino masses are fixed to 0 in this analysis.

5. DISCUSSION

In Section 3 we have shown that the $\text{Ly}\alpha P_{1D}$ can robustly measure two parameters describing the amplitude and slope of the linear power spectrum at a central redshift $z_* = 3$, and around a pivot point $k_* = 0.009 \text{ s km}^{-1}$ defined in velocity units. We have shown that we recover unbiased results independent of the fiducial cosmology assumed in the fits, even when analysing models that were not included in the training of our LaCE emulator.

In Section 4 we have shown that, in the context of joint analyses with CMB data, the cosmological information in the $\text{Ly}\alpha P_{1D}$ can be captured with the marginalised posteriors of these two parameters. We have explicitly shown that this is the case for the two single-parameter extensions to the ΛCDM model where the P_{1D} is forecasted to contribute the most (Font-Ribera et al. 2014): models with massive neutrinos (Figure 3) and models with running of the spectral index of primordial fluctuations (Figure 4).

The compression is successful as we are able to approximate the expansion and growth rates in the $2 < z < 5$ regime using a fixed fiducial model, due to the fact that the Universe is close to Einstein de-Sitter in this regime. At significantly higher data precision, one would expect

this approximation to break down, and therefore the compression to fail. In this case, including the extended parameters discussed in C might capture the missing information. However, the data covariance we use in this work will not be surpassed by any current or proposed experiment, so we leave quantifying the regime in which the compression fails to a future work.

Exotic cosmological models might require more complex implementations of the emulation and compression schemes discussed in this work. For instance, models with either warm or fuzzy dark matter predict that the linear power spectrum could be strongly suppressed on sub-megaparsec scales, and the $\text{Ly}\alpha$ forest has provided some of the tightest constraints on these models (Viel et al. 2013; Iršič et al. 2017b,a; Murgia et al. 2018; Palanque-Delabrouille et al. 2020; Rogers & Peiris 2021b). In order to use the LaCE emulator in these studies, one would need to add extra emulator parameters describing the suppression of the linear power, and run extra simulations exploring them. Equivalently to Δ_*^2 and n_* , one would need to define other *compressed* parameters to capture the relevant information present in the P_{1D} likelihood. Since the P_{1D} measurements are naturally carried out in velocity units, these extra pa-

rameters would also need to be defined in velocity units, otherwise the cutoff scale would depend on the assumed model of the expansion rate $H(z)$.

In the next few years, the Dark Energy Spectroscopic Instrument (DESI) will measure with unprecedented accuracy the Ly α P_{1D} , enabling very precise constraints on the linear power spectrum of matter fluctuations around $z = 3$. We expect that the compression scheme discussed here will significantly increase the impact of these measurements, and it will simplify joint analyses with external datasets.

1 The authors thank Patrick McDonald, Pablo Lemos
 2 Portela, and the Ly α working group of DESI for use-
 3 ful discussions. CP acknowledges support by NASA
 4 ROSES grant 12-EUCLID12-0004. AFR acknowledges
 5 support from the Spanish Ministry of Science and In-
 6 novation through the program Ramon y Cajal (RYC-
 7 2018-025210) and from the European Union’s Horizon
 8 Europe research and innovation programme (COSMO-
 9 LYA, grant agreement 101044612). IFAE is partially
 10 funded by the CERCA program of the Generalitat de
 11 Catalunya. This manuscript has been co-authored by
 12 Fermi Research Alliance, LLC under Contract No. DE-
 13 AC02-07CH11359 with the U.S. Department of Energy,
 14 Office of Science, Office of High Energy Physics. This
 15 work was partially supported by the Visiting Schol-
 16 ars Award Program of the Universities Research As-
 17 sociation, and by funding from the UCL Cosmopar-
 18 ticle Initiative. This work used computing facilities
 19 provided by the UCL Cosmoparticle Initiative. The
 20 simulations were run using the Cambridge Service for
 21 Data Driven Discovery (CSD3), part of which is oper-
 22 ated by the University of Cambridge Research Com-
 23 puting on behalf of the STFC DiRAC HPC Facility
 24 (www.dirac.ac.uk). The DiRAC component of CSD3
 25 was funded by BEIS capital funding via STFC capi-
 26 tal grants ST/P002307/1 and ST/R002452/1 and STFC
 27 operations grant ST/R00689X/1. DiRAC is part of the
 28 National e-Infrastructure.

APPENDIX

A. IMPACT OF PRIOR CHOICE

The results presented in the main text used a Gaussian prior described in Table 2. In Figure 5 we demonstrate that the marginalised posteriors for the compressed parameters are not affected by this prior.

We start by showing the results from a direct analysis (blue contours) and a template analysis (red contours) that include the Gaussian prior; these are the contours already presented in the top right panel of Figure 1. These can be compared respectively to the black and green dotted contours, where we have not included the Gaussian prior.

B. IMPACT OF COSMIC VARIANCE IN THE EMULATOR PREDICTIONS

In the main text we have analysed simulations that had initial conditions generated with the same random phases than the simulations used to train the LaCE emulator. In order to study the impact of cosmic variance in the emulator predictions, in 6 we show the results when analysing a test simulation *diff seed* (red contours) that has the same physics than the *Central* simulation (blue contours), but has different random phases in the initial conditions.

In the same figure we also compare the results when using two different implementations of the LaCE emulator: the *polyfit* framework (solid lines), used in the main text, emulates the value of the coefficients of polynomial fits describing the Ly α P_{1D} (Equation 1); the *k_bin* framework (dotted lines), used in Pedersen et al. (2021), directly emulates the value of Ly α P_{1D} on a fine grid of wavenumbers.

It is clear that the *k_bin* emulator gives biased results, probably because it is trying to fit different noise spikes than the ones used in the training sample. On the other hand, the *polyfit* emulator is able to give unbiased results even when analysing mock data with different cosmic variance.

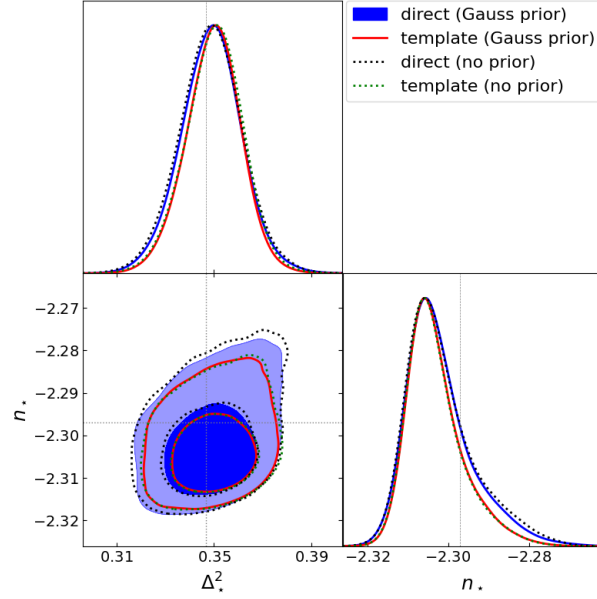


Figure 5. Marginalised 1D and 2D posterior distributions on compressed parameters, corresponding to analyses of the *Central* mock data. In blue we show the constraints from a direct P_{1D} analysis using the loose Gaussian priors, and in red we show the constraints from an equivalent template fit (fixed values for ω_c , H_0 and Σm_ν); these 2D contours were already presented in the top right panel of Figure 1. The black (green) dotted contours show the constraints from a direct (template) fit when not using any Gaussian prior, and demonstrate that the role of the Gaussian prior on the compressed constraints is very minor.

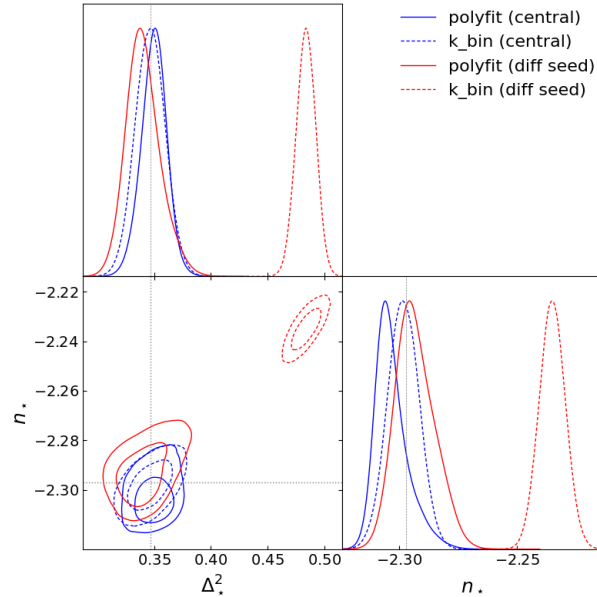


Figure 6. Marginalised 1D and 2D posterior distributions on compressed parameters, corresponding to template fits to the *Central* mock data (in blue) discussed in Figure 1, and fits to mock data with different random phases (diff seed, in red). In solid lines show the constraints when using the *polyfit* framework used in the main text, where we emulate the coefficients of polynomial fits to P_{1D} . The dotted lines, on the other hand, use the *k_bin* framework that was used in Pedersen et al. (2021), where we emulate the value of P_{1D} on a grid of wavenumbers. While both frameworks give consistent results when analysing the *Central* simulation, it is clear that the *k_bin* emulator gives biased results when analysing simulations with different random phases (dotted red contours).

C. EXTENDED COMPRESSION SCHEMES

In Section 3 we have proposed to compress the cosmological information in P_{1D} into two parameters describing the amplitude (Δ_\star^2) and slope (n_\star) of the linear power spectrum at $z_\star = 3$, around a pivot point $k_\star = 0.009 \text{ s km}^{-1}$. We have shown in Section 4 that this compression is lossless in the context of joint analyses with the CMB with free neutrino masses (Σm_ν), or free running of the primordial power spectrum (α_s). In Section 5 we mentioned that one might need to add extra parameters describing the shape of the linear power at z_\star . For instance, a third parameter describing the curvature around the pivot point (McDonald et al. 2005), or a cut-off to describe the small-scales suppression in non-cold dark matter models. In this appendix, instead, we discuss possible extensions to capture other cosmological information beyond the shape of the linear power at z_\star .

Measurements of the Ly α P_{1D} typically cover a wide range of redshifts. For instance, Chabanier et al. (2019b) measured P_{1D} from $z = 2.2$ to $z = 4.6$. It might seem surprising that we can capture all the cosmological information when parameterising the linear power spectrum at a single redshift $z_\star = 3$. Moreover, while the shape of the linear power spectrum is constant when described in comoving units, the same is not true when described in velocity units. Our pivot scale k_\star correspond to different comoving separations at different redshifts, and one could imagine measuring $H(z)/(1+z)$ from the redshift evolution of the shape of the linear power in velocity units.

In order to capture information from these two effects, we introduce two extra parameters. We parameterise the growth of structure around z_\star with the logarithmic growth rate $f_\star = f(z_\star)$, defined as usual:

$$f(z) = \frac{\partial \ln D(z)}{\partial \ln a(z)}, \quad (\text{C1})$$

with $f_\star = 1$ in an Einstein-de Sitter (EdS) universe.

Similarly, we parameterise the evolution of the expansion rate around z_\star in terms of $g_\star = g(z_\star)$, defined as:

$$g(z) = \frac{\partial \ln H(z)}{\partial \ln(1+z)^{3/2}}, \quad (\text{C2})$$

such that $g_\star = 1$ corresponds again to an EdS universe.

C.1. Template fits with f_\star and g_\star

Instead of looking at posteriors of f_\star and g_\star computed as derived parameters in fits for a particular model, we would like to directly sample these without assuming any cosmological model. For instance, in a Λ CDM universe, without curvature or massive neutrinos, both f_\star and g_\star would be just a function of Ω_m . However, more exotic models could decouple the linear growth from the expansion of the universe, making these parameters independent.

Therefore, in this appendix we directly sample the four compressed parameters (Δ_\star^2 , n_\star , f_\star , g_\star) and the same eight nuisance parameters used in the main text to model the IGM. We use a uniform prior range of $[0.24, 0.47]$, $[-2.352, -2.25]$, $[0.9, 1.0]$, $[0.9, 1.0]$ for each parameter respectively. The details of how we do this are detailed later in Section C.2.

In figure 7 we show constraints on compressed parameters, after marginalising over the IGM. We use as a mock dataset the *Neutrino* simulation, and show two sets of constraints. In red, we have fixed f_\star and g_\star to the values of the fiducial cosmology ($f_\star = 0.981$, $g_\star = 0.968$), whereas in blue they are left as free parameters. The dashed lines show the true values in the mock simulation ($f_\star = 0.989$, $g_\star = 0.969$). We note that f_\star is very poorly constrained, implying that the P_{1D} alone is not highly sensitive to the redshift evolution of the linear power spectrum. This result is consistent with the findings of McDonald et al. (2005), although we confirm that this is still the case when using high precision datasets. The posterior for g_\star is slightly better constrained, although it can only rule out very low values of $g_\star < 0.9$. Additionally there is very little effect on the posteriors for Δ_\star^2 and n_\star when marginalising over f_\star and g_\star when compared to fixing them.

Note that the red contours were constructed assuming the wrong background cosmology (wrong values of f_\star and g_\star), but that the constraints on Δ_\star^2 and n_\star are nevertheless unbiased.

C.2. Reconstructing the linear power spectrum

Here we describe the procedure for mapping from a set of values for the compressed parameters (Δ_\star^2 , n_\star , f_\star , g_\star) to the 11 pairs of emulator parameters (Δ_p^2 , n_p) values required to generate theoretical predictions for the P_{1D} from

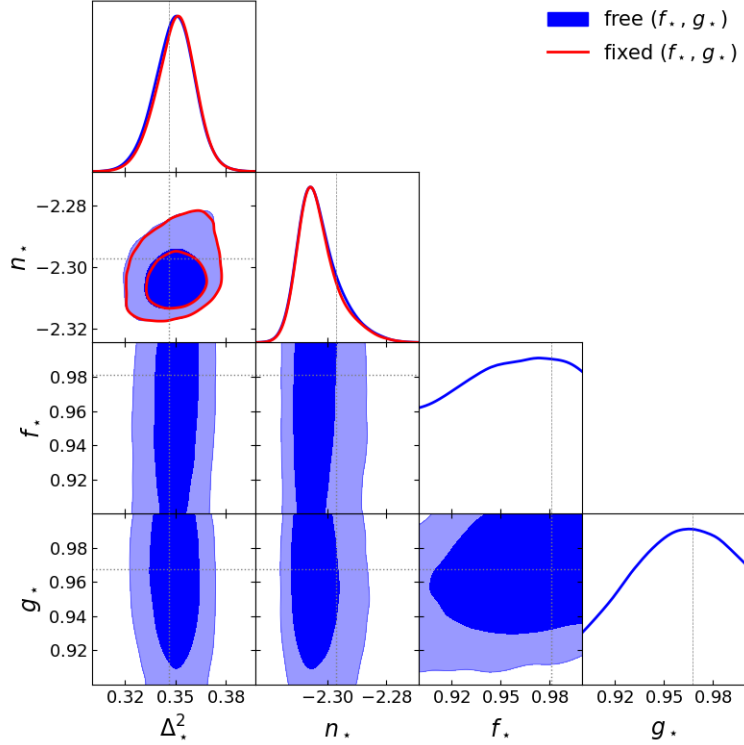


Figure 7. Marginalised 1D and 2D posterior distributions on compressed parameters when analysing the mock dataset from the *Neutrino* simulation. In the red contours we fix f_* and g_* to the fiducial values described in the text. The dashed lines show the true values in the mock simulation, and the shaded areas of the 1D posteriors show the 68% credible region.

the emulator, one at each redshift. This is done using a fiducial cosmology, as outlined below. We will use k to refer to the (modulus of the) 3D wavenumbers in comoving coordinates, i.e., in Mpc. We will use q to refer to the same wavenumber in velocity units. They are related by:

$$k = \frac{H(z)}{1+z} q = M(z) q . \quad (\text{C3})$$

$M(z)$ will play an important role in this discussion.

We will use $P(k)$ to refer to (3D) power spectra in comoving units, i.e., with units of Mpc^3 . We will use $Q(q)$ to refer to (3D) power spectra in velocity units, i.e., with units of $(\text{kms}^{-1})^3$. They are related by:

$$Q(z, q) = M^3(z) P(z, k = M(z)q) . \quad (\text{C4})$$

In our code we will use a fiducial cosmology as a reference, and parameterise our models as deviations from that cosmology. We will use either subscripts $_0$ or superscripts 0 to identify functions for the fiducial cosmology. We address changes to the shape of the power spectrum, as described by Δ_*^2 , n_* (and α_*) first, and then later address changes to the redshift evolution using f_* and g_* . We can now define the ratio of the linear power between any model and the fiducial one, at the central redshift z_* , and in velocity units:

$$B(q) = \frac{Q_*(q)}{Q_*^0(q)} . \quad (\text{C5})$$

This will be another important function, tightly related to the linear power parameters that we will end up using.

We fit a second order polynomial to the logarithm of the linear power spectrum at z_* , in velocity units, around a pivot point q_* . By default we use $z_* = 3$ and $q_* = 0.009$ s/km, and we fit the polynomial in a range of wavenumbers defined as $q_*/2 < q < 2q_*$ ¹².

$$Q_*(q) \approx A \left(\frac{q}{q_*} \right)^{n_* + \alpha_*/2 \ln(q/q_*)}, \quad (\text{C6})$$

or equivalently

$$\ln Q_*(q) \approx \ln A + [n_* + \alpha_*/2 \ln(q/q_*)] \ln(q/q_*). \quad (\text{C7})$$

n_* is the first log-derivative around q_* , and α_* is the second log-derivative around the same point. Note that the polynomial fit, however, returns $(\ln A, n_*, \alpha_*/2)$. Finally, we define a dimensionless parameter describing the amplitude, $\Delta_*^2 = A q_*^3 / (2\pi^2)$. When reconstructing the linear power spectrum using a fiducial cosmology, we use differences in the shape parameters with respect to the fiducial ones:

$$\begin{aligned} \ln B(q) &= \ln Q_*(q) - \ln Q_*^0(q) \\ &\approx (\Delta_*^2 - \Delta_*^2{}^0) + \left[(n_* - n_*^0) + \frac{\alpha_* - \alpha_*^0}{2} \ln(q/q_*) \right] \ln(q/q_*). \end{aligned} \quad (\text{C8})$$

We are also concerned with reconstructing the linear power spectrum at redshifts other than z_* . We ignore neutrinos for now, and work with just the CDM+baryon power spectrum. In this case we can use the linear growth factor $D(z)$, defined as

$$P(z, k) = \left[\frac{D(z)}{D_*} \right]^2 P_*(k), \quad (\text{C9})$$

where in general functions $y_* = y(z_*)$. We can write the power spectrum at an arbitrary redshift as a function of the fiducial one:

$$\begin{aligned} Q(z, q) &= M^3(z) P(z, k = M(z)q) \\ &= M^3(z) \left[\frac{D(z)}{D_*} \right]^2 P_*(k = M(z)q) \\ &= \left[\frac{M(z)}{M_*} \right]^3 \left[\frac{D(z)}{D_*} \right]^2 Q_*(q' = M(z)/M_*q) \\ &= \left[\frac{M(z)}{M_*} \right]^3 \left[\frac{D(z)}{D_*} \right]^2 B(q' = M(z)/M_*q) Q_*^0(q' = M(z)/M_*q) \\ &= \left[\frac{M(z)}{M_*} \right]^3 \left[\frac{D(z)}{D_*} \right]^2 B(q' = M(z)/M_*q) [M_*^0]^3 P_*^0(k = M_*^0 M(z)/M_*q) \\ &= \left[\frac{M(z)}{M_*} \right]^3 \left[\frac{D(z)}{D_*} \right]^2 B(q' = M(z)/M_*q) [M_*^0]^3 \left[\frac{D_*^0}{D_0(z)} \right]^2 P^0(z, k = M_*^0 M(z)/M_*q) \\ &= \left[\frac{M(z)}{M_*} \right]^3 \left[\frac{D(z)}{D_*} \right]^2 B(q' = M(z)/M_*q) \left[\frac{M_*^0}{M_0(z)} \right]^3 \left[\frac{D_*^0}{D_0(z)} \right]^2 Q^0(z, q' = (M_*^0 M(z))/(M_* M_0(z))q) \\ &= [m(z)]^3 [d(z)]^2 B(q' = m(z)M_0(z)/M_*^0q) Q^0(z, q' = m(z)q), \end{aligned}$$

where for convenience we have defined two functions,

$$m(z) = \frac{M(z)}{M_*} \frac{M_*^0}{M_0(z)} \quad (\text{C10})$$

and

$$d(z) = \frac{D(z)}{D_*} \frac{D_*^0}{D_0(z)}, \quad (\text{C11})$$

¹² We do the fit using `numpy.polyfit`

that describe differences in expansion rate and in linear growth respectively.

Using the definition of g_* in Equation C2, we approximate $m(z)$ using the difference of g_* between the input and the fiducial cosmology as:

$$\ln m(z) \approx \frac{3}{2} (g_* - g_*^0) \ln \left(\frac{1+z}{1+z_*} \right), \quad (\text{C12})$$

or equivalently

$$m(z) \approx \left(\frac{1+z}{1+z_*} \right)^{3/2(g_* - g_*^0)}. \quad (\text{C13})$$

Similarly, we approximate $d(z)$ using the difference of f_* between the input and the fiducial cosmology as:

$$\ln d(z) \approx - (f_* - f_*^0) \ln \left(\frac{1+z}{1+z_*} \right), \quad (\text{C14})$$

or equivalently

$$d(z) \approx \left(\frac{1+z}{1+z_*} \right)^{-(f_* - f_*^0)}. \quad (\text{C15})$$

With these equations, for a given set of $(\Delta_*^2, n_*, \alpha_*, f_*, g_*)$, $Q(z, q)$ can be estimated. We then use the approximation of $m(z)$ to convert the velocity unit power spectrum to a comoving power spectrum, and fit a polynomial over the range $k_p/2 < k < 2k$ to obtain values for Δ_p^2 and n_p . Note that the emulator returns a P_{ID} in comoving units. The final step is to convert this into velocity units, once again using the above approximation of $m(z)$. This reconstruction process and the composite approximations have been compared against the true values generated in CAMB, and we verified that they are accurate to within the percent level across all redshifts and extended model spaces considered in this paper.

REFERENCES

- Abbott, T. M. C., Agüena, M., Alarcon, A., et al. 2022, *Phys. Rev. D*, 105, 023520, doi: [10.1103/PhysRevD.105.023520](https://doi.org/10.1103/PhysRevD.105.023520)
- Aghamousa, A., & et al. ????, <https://www.osti.gov/biblio/1345632>
- Alam, S., Aubert, M., Avila, S., et al. 2021, *Phys. Rev. D*, 103, 083533, doi: [10.1103/PhysRevD.103.083533](https://doi.org/10.1103/PhysRevD.103.083533)
- Anderson, L., Pontzen, A., Font-Ribera, A., et al. 2019, *ApJ*, 871, 144, doi: [10.3847/1538-4357/aaf576](https://doi.org/10.3847/1538-4357/aaf576)
- Angulo, R. E., & Pontzen, A. 2016, *MNRAS*, 462, L1, doi: [10.1093/mnrasl/slw098](https://doi.org/10.1093/mnrasl/slw098)
- Bird, S. 2017, FSFE: Fake Spectra Flux Extractor, Astrophysics Source Code Library, <http://ascl.net/1710.012>
- Bird, S., Peiris, H. V., Viel, M., & Verde, L. 2011, *MNRAS*, 413, 1717, doi: [10.1111/j.1365-2966.2011.18245.x](https://doi.org/10.1111/j.1365-2966.2011.18245.x)
- Bird, S., Rogers, K. K., Peiris, H. V., et al. 2019, *JCAP*, 2019, 050, doi: [10.1088/1475-7516/2019/02/050](https://doi.org/10.1088/1475-7516/2019/02/050)
- Borde, A., Palanque-Desabrouille, N., Rossi, G., et al. 2014, *Journal of Cosmology and Astro-Particle Physics*, 2014, 005, doi: [10.1088/1475-7516/2014/07/005](https://doi.org/10.1088/1475-7516/2014/07/005)
- Brieden, S., Gil-Marín, H., & Verde, L. 2021, *JCAP*, 2021, 054, doi: [10.1088/1475-7516/2021/12/054](https://doi.org/10.1088/1475-7516/2021/12/054)
- Chabanier, S., Millea, M., & Palanque-Desabrouille, N. 2019a, *MNRAS*, 489, 2247, doi: [10.1093/mnras/stz2310](https://doi.org/10.1093/mnras/stz2310)
- Chabanier, S., Palanque-Desabrouille, N., Yèche, C., et al. 2019b, *JCAP*, 2019, 017, doi: [10.1088/1475-7516/2019/07/017](https://doi.org/10.1088/1475-7516/2019/07/017)
- Croft, R. A. C., Weinberg, D. H., Bolte, M., et al. 2002, *ApJ*, 581, 20, doi: [10.1086/344099](https://doi.org/10.1086/344099)
- Croft, R. A. C., Weinberg, D. H., Katz, N., & Hernquist, L. 1998, *ApJ*, 495, 44, doi: [10.1086/305289](https://doi.org/10.1086/305289)
- d’Amico, G., Gleyzes, J., Kokron, N., et al. 2020, *JCAP*, 2020, 005, doi: [10.1088/1475-7516/2020/05/005](https://doi.org/10.1088/1475-7516/2020/05/005)
- Dawson, K. S., Schlegel, D. J., Ahn, C. P., et al. 2013, *AJ*, 145, 10, doi: [10.1088/0004-6256/145/1/10](https://doi.org/10.1088/0004-6256/145/1/10)
- Dawson, K. S., Kneib, J.-P., Percival, W. J., et al. 2016, *AJ*, 151, 44, doi: [10.3847/0004-6256/151/2/44](https://doi.org/10.3847/0004-6256/151/2/44)
- du Mas des Bourboux, H., Rich, J., Font-Ribera, A., et al. 2020, *ApJ*, 901, 153, doi: [10.3847/1538-4357/abb085](https://doi.org/10.3847/1538-4357/abb085)
- Feng, Y., Bird, S., Anderson, L., Font-Ribera, A., & Pedersen, C. 2018, MP-Gadget/MP-Gadget: A tag for getting a DOI, doi: [10.5281/zenodo.1451799](https://doi.org/10.5281/zenodo.1451799)
- Font-Ribera, A., McDonald, P., Mostek, N., et al. 2014, *JCAP*, 2014, 023, doi: [10.1088/1475-7516/2014/05/023](https://doi.org/10.1088/1475-7516/2014/05/023)

- Foreman-Mackey, D., Hogg, D. W., Lang, D., & Goodman, J. 2013, *Publications of the Astronomical Society of the Pacific*, 125, 306, doi: [10.1086/670067](https://doi.org/10.1086/670067)
- Gnedin, N. Y., & Hamilton, A. J. S. 2002, *MNRAS*, 334, 107, doi: [10.1046/j.1365-8711.2002.05490.x](https://doi.org/10.1046/j.1365-8711.2002.05490.x)
- GPy. since 2012, GPy: A Gaussian process framework in python, <http://github.com/SheffieldML/GPy>
- Haardt, F., & Madau, P. 2012, *ApJ*, 746, 125, doi: [10.1088/0004-637X/746/2/125](https://doi.org/10.1088/0004-637X/746/2/125)
- Hamann, J., Hannestad, S., Lesgourgues, J., Rampf, C., & Wong, Y. Y. Y. 2010, *JCAP*, 2010, 022, doi: [10.1088/1475-7516/2010/07/022](https://doi.org/10.1088/1475-7516/2010/07/022)
- Iršič, V., Viel, M., Haehnelt, M. G., Bolton, J. S., & Becker, G. D. 2017a, *PhRvL*, 119, 031302, doi: [10.1103/PhysRevLett.119.031302](https://doi.org/10.1103/PhysRevLett.119.031302)
- Iršič, V., Viel, M., Haehnelt, M. G., et al. 2017b, *Phys. Rev. D* , 96, 023522, doi: [10.1103/PhysRevD.96.023522](https://doi.org/10.1103/PhysRevD.96.023522)
- Ivanov, M. M., Simonović, M., & Zaldarriaga, M. 2020, *JCAP*, 2020, 042, doi: [10.1088/1475-7516/2020/05/042](https://doi.org/10.1088/1475-7516/2020/05/042)
- Lawrence, E., Heitmann, K., White, M., et al. 2010, *ApJ*, 713, 1322, doi: [10.1088/0004-637X/713/2/1322](https://doi.org/10.1088/0004-637X/713/2/1322)
- Lesgourgues, J., & Pastor, S. 2006, *PhR*, 429, 307, doi: [10.1016/j.physrep.2006.04.001](https://doi.org/10.1016/j.physrep.2006.04.001)
- Lewis, A. 2019, arXiv e-prints, arXiv:1910.13970. <https://arxiv.org/abs/1910.13970>
- Lewis, A., Challinor, A., & Lasenby, A. 2000, *ApJ*, 538, 473, doi: [10.1086/309179](https://doi.org/10.1086/309179)
- McDonald, P., Miralda-Escudé, J., Rauch, M., et al. 2000, *ApJ*, 543, 1, doi: [10.1086/317079](https://doi.org/10.1086/317079)
- McDonald, P., Seljak, U., Cen, R., et al. 2005, *ApJ*, 635, 761, doi: [10.1086/497563](https://doi.org/10.1086/497563)
- McQuinn, M. 2016, *ARA&A*, 54, 313, doi: [10.1146/annurev-astro-082214-122355](https://doi.org/10.1146/annurev-astro-082214-122355)
- Murgia, R., Iršič, V., & Viel, M. 2018, *Phys. Rev. D* , 98, 083540, doi: [10.1103/PhysRevD.98.083540](https://doi.org/10.1103/PhysRevD.98.083540)
- Palanque-Delabrouille, N., Yèche, C., Schöneberg, N., et al. 2020, *JCAP*, 2020, 038, doi: [10.1088/1475-7516/2020/04/038](https://doi.org/10.1088/1475-7516/2020/04/038)
- Palanque-Delabrouille, N., Yèche, C., Lesgourgues, J., et al. 2015a, *Journal of Cosmology and Astro-Particle Physics*, 2015, 045, doi: [10.1088/1475-7516/2015/02/045](https://doi.org/10.1088/1475-7516/2015/02/045)
- Palanque-Delabrouille, N., Yèche, C., Baur, J., et al. 2015b, *JCAP*, 2015, 011, doi: [10.1088/1475-7516/2015/11/011](https://doi.org/10.1088/1475-7516/2015/11/011)
- Pedersen, C., Font-Ribera, A., Kitching, T. D., et al. 2020, *JCAP*, 2020, 025, doi: [10.1088/1475-7516/2020/04/025](https://doi.org/10.1088/1475-7516/2020/04/025)
- Pedersen, C., Font-Ribera, A., Rogers, K. K., et al. 2021, *JCAP*, 2021, 033, doi: [10.1088/1475-7516/2021/05/033](https://doi.org/10.1088/1475-7516/2021/05/033)
- Phillips, J., Weinberg, D. H., Croft, R. A. C., et al. 2001, *ApJ*, 560, 15, doi: [10.1086/322369](https://doi.org/10.1086/322369)
- Planck Collaboration, Aghanim, N., Akrami, Y., et al. 2020, *A&A*, 641, A6, doi: [10.1051/0004-6361/201833910](https://doi.org/10.1051/0004-6361/201833910)
- Rogers, K. K., & Peiris, H. V. 2021a, *Phys. Rev. D* , 103, 043526, doi: [10.1103/PhysRevD.103.043526](https://doi.org/10.1103/PhysRevD.103.043526)
- . 2021b, *PhRvL*, 126, 071302, doi: [10.1103/PhysRevLett.126.071302](https://doi.org/10.1103/PhysRevLett.126.071302)
- Rogers, K. K., Peiris, H. V., Pontzen, A., et al. 2019, *JCAP*, 2019, 031, doi: [10.1088/1475-7516/2019/02/031](https://doi.org/10.1088/1475-7516/2019/02/031)
- Seljak, U., Slosar, A., & McDonald, P. 2006, *JCAP*, 2006, 014, doi: [10.1088/1475-7516/2006/10/014](https://doi.org/10.1088/1475-7516/2006/10/014)
- Seljak, U., Makarov, A., McDonald, P., et al. 2005, *Phys. Rev. D* , 71, 103515, doi: [10.1103/PhysRevD.71.103515](https://doi.org/10.1103/PhysRevD.71.103515)
- Spergel, D. N., Verde, L., Peiris, H. V., et al. 2003, *ApJS*, 148, 175, doi: [10.1086/377226](https://doi.org/10.1086/377226)
- Springel, V. 2005, *MNRAS*, 364, 1105, doi: [10.1111/j.1365-2966.2005.09655.x](https://doi.org/10.1111/j.1365-2966.2005.09655.x)
- Takhtaganov, T., Lukić, Z., Müller, J., & Morozov, D. 2021, *ApJ*, 906, 74, doi: [10.3847/1538-4357/abc8ed](https://doi.org/10.3847/1538-4357/abc8ed)
- Verde, L., Peiris, H. V., Spergel, D. N., et al. 2003, *ApJS*, 148, 195, doi: [10.1086/377335](https://doi.org/10.1086/377335)
- Viel, M., Becker, G. D., Bolton, J. S., & Haehnelt, M. G. 2013, *Phys. Rev. D* , 88, 043502, doi: [10.1103/PhysRevD.88.043502](https://doi.org/10.1103/PhysRevD.88.043502)
- Viel, M., Weller, J., & Haehnelt, M. G. 2004, *MNRAS*, 355, L23, doi: [10.1111/j.1365-2966.2004.08498.x](https://doi.org/10.1111/j.1365-2966.2004.08498.x)
- Villaescusa-Navarro, F., Naess, S., Genel, S., et al. 2018, *ApJ*, 867, 137, doi: [10.3847/1538-4357/aae52b](https://doi.org/10.3847/1538-4357/aae52b)
- Virtanen, P., Gommers, R., Oliphant, T. E., et al. 2020, *Nature Methods*, 17, 261, doi: [10.1038/s41592-019-0686-2](https://doi.org/10.1038/s41592-019-0686-2)
- Walther, M., Oñorbe, J., Hennawi, J. F., & Lukić, Z. 2019, *ApJ*, 872, 13, doi: [10.3847/1538-4357/aafad1](https://doi.org/10.3847/1538-4357/aafad1)